Liquid intrusion and alternative methods for the characterization of macroporous materials (IUPAC Technical Report)*

Jean Rouquerol[1,‡], Gino Baron[2], Renaud Denoyel[1],
Herbert Giesche[3], Johan Groen[4], Peter Klobes[5], Pierre Levitz[6],
Alexander V. Neimark[7], Sean Rigby[8], Romas Skudas[9],
Kenneth Sing[10], Matthias Thommes[11], and Klaus Unger[9]

[1]*LCP, CNRS-University Aix-Marseille, Marseille, France;* [2]*Vrije Universiteit Brussels, Brussels, Belgium;* [3]*NYSCC at Alfred University, Alfred, NY, USA;* [4]*Delft Solids Solutions B.V., Delft, The Netherlands;* [5]*BAM Bundesanstalt für Materialforschung und -prüfung, Berlin, Germany;* [6]*Ecole Polytechnique, Palaiseau, France;* [7]*Rutgers University, Piscataway, NJ, USA;* [8]*Bath University, Bath, UK;* [9]*Johannes Gutenberg University, Mainz, Germany;* [10]*Brunel University, Uxbridge, UK;* [11]*Quantachrome Instruments, Boynton Beach, FL, USA*

Abstract: This document deals with the characterization of porous materials having pore widths in the macropore range of 50 nm to 500 µm. In recent years, the development of advanced adsorbents and catalysts (e.g., monoliths having hierarchical pore networks) has brought about a renewed interest in macropore structures. Mercury intrusion–extrusion porosimetry is a well-established method, which is at present the most widely used for determining the macropore size distribution. However, because of the reservations raised by the use of mercury, it is now evident that the principles involved in the application of mercury porosimetry require reappraisal and that alternative methods are worth being listed and evaluated. The reliability of mercury porosimetry is discussed in the first part of the report along with the conditions required for its safe use. Other procedures for macropore size analysis, which are critically examined, include the intrusion of other non-wetting liquids and certain wetting liquids, capillary condensation, liquid permeation, imaging, and image analysis. The statistical reconstruction of porous materials and the use of macroporous reference materials (RMs) are also examined. Finally, the future of macropore analysis is discussed.

Keywords: capillary condensation; image analysis; IUPAC Physical and Biophysical Chemistry Division; liquid intrusion; macroporous materials; mercury porosimetry; permeation; pore size characterization; reference porous materials; statistical reconstruction of porous solids.

CONTENTS

1. INTRODUCTION

The main objective of this document is to review critically the various *liquid intrusion* techniques commonly used to assess the pore size of materials containing macropores (i.e., pores of width >50 nm), especially those in the approximate range 50 nm to 500 µm. Further objectives are to examine the potential value of various other techniques and also the relevant aspects of the general methodology of macropore size analysis. There is now indeed a special need for particular attention to be given to the characterization of *macroporous* materials. For many years physical chemists and others were more concerned with the characterization of *micropores* (of width smaller than 2 nm) and *mesopores* (width between 2 and 50 nm) [1,2]: these pores are generally responsible for the large surface area of many adsorbents and catalysts. The recent development of adsorbents and catalysts in the form of solid "monoliths" has led to the concept of "hierarchical" pore structures, with an appropriate balance of micropores, mesopores, and *macropores*, the latter being required to ensure the transport of the fluids to and from the smaller pores at a satisfactory rate. Hence, a renewed interest in macroporosity among scientists and industrialists working with catalysts, pharmaceuticals, building materials, ancient monuments, tailor-made adsorbents (for chromatography, liquid purification, gas separation, or storage), and biomaterials such as bones or biomedical fibres.

The characterization of macropores involves both *environmental* and *technical* issues. The principal method used at present for macropore size analysis is based on mercury intrusion. Although mercury can be handled, like any other chemical, with appropriate safety measures, it is felt highly desirable to replace mercury porosimetry by some other method more favourable to the environment—even though for the time being there is still no well-established alternative to mercury porosimetry. Any possible replacement raises important technical issues. *This document aims to provide a first step toward satisfactory answers, by listing, examining, and evaluating all trials already made in the field.* As will be seen, these include the intrusion of safer liquids (e.g., other molten metals, water, organics) and also the possible extension of capillary condensation analysis into the macropore range where, for technical reasons, it is often considered inapplicable. However, it is widely recognised that there is also an urgent need to explore and evaluate the application of new techniques for macropore size analysis, and this document, therefore, aims to clarify the essential requirements.

2. MERCURY INTRUSION

2.1 General aspects of mercury porosimetry

Mercury porosimetry is generally accepted as the most useful available method for the textural analysis of macroporous samples (i.e., pores of diameters >50 nm). The main attraction is that it allows the pore size analysis to be undertaken over a wide range of mesopore–macropore widths (routinely, from ca. 0.003 to ca. 400 µm) [3–6]. In addition, mercury porosimetry may provide a means of assessing the surface area and particle size distribution and also investigating the tortuosity, permeability, fractal dimension, and compressibility of porous materials. Furthermore, it is possible to obtain useful information relating to the pore shape, network effects, and the skeletal and bulk density [3,4,6].

In contrast to capillary condensation, where the pore fluid wets the pore walls (i.e., the contact angle is <90º), mercury porosimetry makes use of a non-wetting situation (contact angle >90º), and therefore pressure must be applied to force mercury into the pores. Thus, a progressive increase in hydrostatic pressure is applied to enable the mercury to enter the pores in decreasing order of width. Accordingly, there is an inverse relationship between the applied pressure p and the pore diameter d_p, which in the simplest case of cylindrical pores is given by the Washburn equation

$$d_p = -(4\gamma/p) \cos \theta \qquad (1)$$

where γ is the surface tension of mercury and θ the contact angle between the solid sample and mercury.

To apply eq. 1 for the calculation of d_p, it is necessary to insert values for γ and θ. Generally, γ is assumed to be 484 mN·m^{-1}, which is the surface tension of pure mercury at 25 °C. Strictly speaking, the contact angle θ must depend on the nature of the solid surface. The measurement of θ for a mercury drop lying on a flat surface of a similar solid is a means of evaluating θ, although differences may exist in crystalline structure and purity between the flat surface and the pore wall. These uncertainties make it desirable to distinguish between two goals. First, for routine work or if the objective is to share and compare results with other laboratories, then a standard calculation procedure is desirable and the customary value of 140º can be used. Secondly, in making comparisons with other methods, it may be useful to attempt to adjust the value of θ, but of course this should be clearly recorded.

In the application of mercury porosimetry, the volume of mercury entering the pore structure is measured as the applied (hydrostatic) pressure is gradually increased. The value $v_i(Hg)$ at the applied pressure p_i apparently gives the cumulative volume of all available pores of radius equal to, or greater than, d_p.

With modern commercial equipment, the pressure can be increased from 0.003 to 400 MPa corresponding to cylindrical pore diameters of 400 µm down to 3.6 nm (by assuming a contact angle of 140º). Allowance must be made for the compressibility and thermal effects of mercury, the hydraulic fluid, and the sample, and for thermophysical elastic distortion of the sample cell. Good initial evacuation of the sample, purity of the mercury, and proper choice of equilibration times are also critical for a successful experiment and consequently a reliable textural analysis of the sample.

2.2 Interpretation of a typical mercury intrusion–extrusion measurement

Figure 1 shows two typical intrusion–extrusion cycles for the intrusion and extrusion of mercury as a function of pressure (i.e., as ln p) [6]. Region (a) corresponds to a rearrangement of particles within the powder bed, followed by intrusion into the interparticle voids (b). Filling of the pores occurs in the region (c), and for some materials (reversible) compression is then possible at higher pressures (d). Hysteresis is observed, and extrusion (e) occurs at different pressures than for the intrusion. On completion of a first intrusion–extrusion cycle, some mercury is usually retained by the sample, thereby preventing the loop from closing (f). Intrusion–extrusion cycles after the first continue to show hysteresis (g) but eventually the loop closes, showing that there is no further entrapment of mercury. On most samples, the loop closes after just the second cycle.
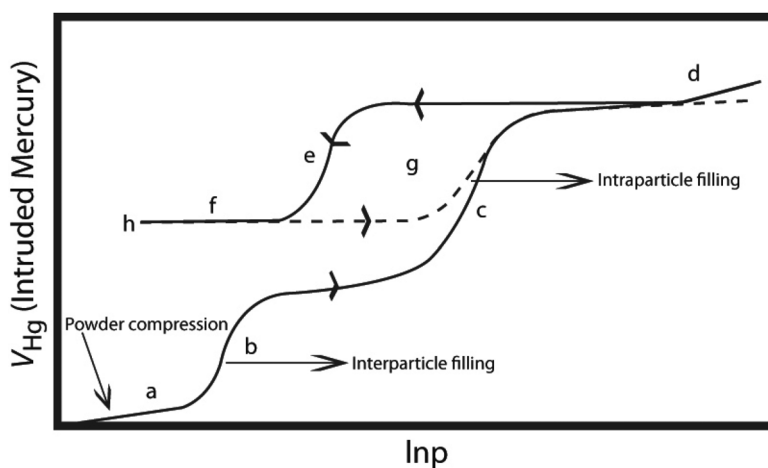

Fig. 1 Recording for two intrusion–extrusion cycles of mercury.

An understanding of the hysteresis and entrapment phenomena is most important in order to obtain a comprehensive pore size analysis. Experiments with model pore networks and molecular simulation studies appear to confirm that mercury entrapment is caused by the rupture of the mercury in pore constrictions or junctions during extrusion [8,9]. Entrapment and hysteresis are in principle of different origin (as indicated by the fact that intrusion–extrusion cycles after the first continue to show hysteresis but no entrapment, as illustrated in Fig. 1). Various mechanisms have been proposed to explain intrusion–extrusion hysteresis [7–9]. The single-pore mechanism implies that hysteresis is an intrinsic property of the intrusion–extrusion process owing either to a nucleation barrier associated with the formation of the vapour–liquid interface during extrusion or to a difference in the advancing and receding contact angles. The network models take into account both ink-bottle and percolation effects in pore networks. It is now generally accepted that pore blocking, which can occur on the intrusion branch, is somewhat similar to the percolation effects involved in gas desorption from porous networks. Pore blocking is the dominant mechanism in disordered pore networks, and in this case a reliable pore size distribution can only be calculated from the intrusion branch by applying complex network models based on percolation theory. With certain systems, the application of such models also allows one to obtain a limited amount of structural information from the intrusion–extrusion hysteresis loop [7,8].

It is noteworthy that the general shape of a mercury intrusion–extrusion hysteresis loop is often remarkably similar to that of the corresponding gas adsorption loop. Thus, mercury intrusion and capillary evapouration appear to follow similar pathways. This has been confirmed in recent work in which the behaviour of wetting and non-wetting fluids in porous solids has been studied by the application of molecular simulation. This microscopic approach based on statistical mechanics has provided a molecular theory of mercury porosimetry and also a unified framework for understanding both gas adsorption and mercury porosimetry [9].

Summarizing, one can state that significant progress has been made in the fundamental understanding of the underlying mechanisms of mercury intrusion–extrusion. Further progress is likely to depend on the further refinement of the theoretical principles and their application to model pore structures.

2.3 Practical recommendations

Mercury porosimetry is still considered to be the standard method for the analysis of the macropore structure of catalysts and supports. In general, the derived values of pore size and pore volume are repeatable to better than 1 % standard deviation. In some cases, the mercury porosimetry data are also in satisfactory agreement with the results obtained by other methods. However, the pore size distribution generated by mercury porosimetry is primarily useful in comparative studies of similar materials. It must be kept in mind that the accuracy of the porosity data is dependent on various assumptions and experimental factors, some of which are not easy to take into account. The following points should be taken into account when mercury porosimetry is used for pore size analysis:

- In the case of materials consisting of complex pore networks, the position of the intrusion branch is governed by the size of pore entrances, but not the overall pore size. In addition, the assumption that the material consists of an assembly of independent pores with a certain well-defined geometry is questionable for disordered materials.
- The largest measurable pore size is limited by the height of the sample, i.e., the residual hydrostatic pressure of mercury at the bottom of a 1-cm-high sample already fills the pores larger than 1 mm.
- It is strongly recommended that the measurements should not be restricted to the determination of an intrusion curve alone because it is possible to identify certain distinctive features of the intrusion–extrusion behaviour. Reproducibility of the hysteresis loop in a second intrusion–extrusion cycle indicates that the structure of the samples was not irreversibly affected in the first cycle

(i.e., there was no fracture of the material) and gives additional information about the texture of the material. Scanning the hysteresis loop in combination with the application of advanced network models can also provide information about the pore network and the solid structure.

- As already discussed in connection with Fig. 1, in the case of powders the application of mercury porosimetry often allows one to distinguish between interparticle voids and intraparticle pores. In principle, analysis of the interparticle intrusion provides an indication of the particle size distribution, but in practice there may be a significant overlap of intrusion. In addition, the effect of powder compaction or rearrangement has to be taken into account (see Fig. 1), which usually occurs at relatively low pressures as the mercury penetrates into large interparticle voids.
- Owing to the high pressures involved in mercury porosimetry, elastic or permanent structural changes may occur in highly porous or "soft" materials. The opposite effect may also occur when materials are stacked (layered) in the sample cell, with the result that interparticle pores that were not in the starting material are created. Thus, by the alignment of very thin layers of material under pressure, new slit-shaped pores can form between the layers.
- Some metals or alloys form amalgams when in contact with mercury, which leads to a dramatic change of the contact angle. Fortunately, in most cases a thin oxide layer or other surface contaminants retard the amalgamation to such a degree that no further protective steps (e.g., stearic acid coating) are required.

2.4 Safety recommendations

Mercury should be handled with the same care that any other laboratory chemical is given. The current Occupational Safety and Health Administration (OSHA) permissible exposure limit (PEL) for mercury vapour is 0.1 mg·m^{-3} of air [10]. The National Institute for Occupational Safety and Health (NIOSH) has established (in 2004) a recommended exposure limit (REL) for mercury vapour of 0.05 mg·m^{-3} as a time-weighted average (TWA) for up to a 10-h workday and a 40-h workweek [12]. The following links [11–13] provide information about safe handling of mercury in the United States. However, it is strongly recommended that the appropriate specific regulations and recommendations for the country should be checked. Safe working conditions are quite easy to maintain if a few simple guidelines are followed:

- Use appropriate personal protective clothing and equipment effective in preventing skin contact with mercury.
- Always work with mercury over a spill tray. Keep all containers with mercury sealed when not in use. Waste mercury in any work area must be in spill trays covered with oil.
- Ensure that containers of mercury are securely capped when not actually being poured from, or into. Handle containers of mercury, including sample cells, in a well-ventilated area. Mercury porosimeter measurement cells should be cleaned in a fume hood.
- Use the mercury vapour traps supplied on the equipment and never override or disable any safety device.
- If at all possible, any operation with mercury should be performed in a separate room with proper ventilation and no "lab traffic". The use of a so-called "Tacky Mat" placed outside the mercury test area, on which mercury porosimeter users must step with both feet when exiting the mercury test area, is also recommended.

Under normal operating conditions, the above-stated RELs should never be reached. However, it is advisable to check periodically the actual concentration, for instance, by monitor badges that are worn by the operator. This test should be performed at least annually, but always after a spill has occurred. All mercury spills should be cleaned immediately and thoroughly by mechanical, chemical, or other appropriate means.

Anyone dealing with the clean-up should wear a respirator and, of course, protective clothing to prevent any skin contact with mercury.

It is not only from an environmental standpoint that it is important to stress that used mercury should be recycled. It can be sent to an appropriate institution or company that specializes in the recycling of mercury. Re-distilled (i.e., triple-distilled) mercury can be used again in mercury porosimetry applications.

3. INTRUSION OF OTHER NON-WETTING LIQUIDS

3.1 Intrusion of liquid metals

To take advantage of the intrusion porosimetry technique, it may seem logical to replace mercury by another, less hazardous, non-wetting metal that is liquid at room temperature.

At first sight, gallium, indium, and their alloys seem to be possible candidates. Gallium, which melts ca. 30 °C, has indeed a very low vapour pressure and for this reason would be much less harmful than mercury. However, it wets a number of oxides and penetrates the crystalline network of most metals, so that it is not suited for a method where the intrusion is controlled only by the applied pressure.

Indium melts at a much higher temperature (156 °C) but can be used to make alloys with lower melting points. For instance, the alloy "Galinstan" (after its components gallium, indium, and tin, respectively), which replaces mercury in thermometers, melts at –19 °C. (Galinstan is a registered trademark of the German company Geratherm Medical AG). Because of its high gallium content, it has similar wetting properties to gallium and is therefore not suitable.

Wood's metal (an alloy of bismuth containing lead, tin, and cadmium) is another possible candidate. It has the advantage of not wetting oxides and rocks, but it only melts at 70 °C, and at that temperature the lead and cadmium it contains are known to be harmful either in the liquid state or in the vapour phase. A nontoxic alternative to Wood's metal is possibly Field's metal (a eutectic alloy of bismuth, indium, and tin), which melts at a lower temperature (62 °C) but is, unfortunately, a wetting liquid.

It therefore seems that there is no readily available metal or metallic alloy capable of replacing mercury in liquid intrusion porosimetry since a useful alternative must be (i) non-wetting on many materials, (ii) liquid at room temperature, and (iii) safer to handle than mercury.

3.2 Water intrusion in hydrophobic materials

Water intrusion in hydrophobic materials has been studied by various groups [14–17]. In principle, this approach could be used in the same way as mercury intrusion to derive the pore size.

However, in practice a number of complicating factors must be taken into account. First, only a minority of macroporous materials are strictly hydrophobic (i.e., for most materials the contact angle is less than 90º). Second, the hydrophilic–hydrophobic behaviour is generally strongly dependent on the surface chemistry and the corresponding water contact angle is usually unknown. In principle, these limitations could be overcome by some form of preliminary surface modification (such as surface grafting of siloxane functional groups), but this entails additional sample preparation.

Water intrusion experiments have been carried out on certain grafted silicas and hydrophobic zeolites such as silicalite [18] and also some carbon surfaces. However, this work was related to the design of small devices for energy storage and mechanical damping, and the materials examined were mainly microporous or mesoporous. Similar studies of macroporous materials would be possible, but would require good control and monitoring of pressures only slightly above the saturation pressure of water.

4. CAPILLARY CONDENSATION EQUILIBRIA OBTAINED THROUGH DRAINAGE AND/OR EVAPORATION

4.1 Liquid porosimetry

While mercury porosimetry remains the primary method for macropore size analysis, increasing concern about the use of mercury calls for the development of alternative techniques based on nontoxic fluids. The most advanced is probably *liquid porosimetry* as developed by Miller and Tyomkin [19], which can utilize any wetting fluid: pure water, water solution of a given surface tension, organic liquids like hexane and decane, etc.

The principle of liquid porosimetry is similar to that of mercury porosimetry, with the only difference that instead of positive pressures required to intrude non-wetting mercury into the pores, one has to apply negative pressures to drain wetting fluid out of the pores. The sample in a test chamber is exposed to the varying and precisely controlled air pressure. The size (radius) of the largest pore able to hold liquid is a function of the external pressure, according to the Young–Laplace equation. As the air pressure is changed, liquid is progressively drained from groups of pores and the pore volume of each group is equal to the volume of transferred liquid, the latter being measured gravimetrically. This method is suitable for the determination of the pore size distribution in the range from 1 to 1000 µm.

This type of liquid porosimetry is a nondestructive technique as opposed to mercury porosimetry. It can be applied to a wide variety of materials, including soft and deformable solids and polymer composites, powders, woven and nonwoven fabrics, and amalgamating metals, which cannot be studied by mercury porosimetry. The method provides a way of assessing the surface area, pore volume, and pore size distribution and the actual uptakes and retention capillary pressures (known as the Leveret functions employed for the computation of two-phase flows in porous media). By using well-characterized reference porous materials, liquid uptake–drainage hysteresis and the effective advancing and receding contact angles in different size pores can be investigated. Further modifications of the method have included the addition of a sample thickness gauge to measure the sample deformation in the process of absorption and drainage and also the characterization of a sample constricted to a fixed thickness or kept under a fixed external load. In this manner, it is possible to investigate the behaviour of sandwiched or laminated structures and liquid partitioning between the contacting porous layers.

4.2 Contact porosimetry

As already indicated, liquid porosimetry can be applied to nonrigid or soft materials in the range of effective pore size above 1 µm. The assessment of smaller pore sizes is hindered by significant technical difficulties. The development of a nondestructive method for macropore characterization in the macropore range below 1 µm is an important practical problem. Its solution is critical for a better understanding of wetting and transport phenomena in porous media, particularly in papers, films, ultrafine filters, membranes, fibrous materials, soil, etc.

A method, which has no apparent restrictions of the pore sizes, is *contact or standard porosimetry*, which was first proposed by Russian scientists, see reviews [20,21]. The method is based on the gravimetric measurements of the content of a liquid in the sample and simultaneously in an attached porous material under conditions of capillary equilibrium. The amount of liquid in the reference solid is varied by impregnation and drainage as well as by condensation and evaporation. In contact with the sample, equilibration is attained via the liquid and gas phases. At thermodynamic equilibrium, the liquid in the contacting porous material has the same chemical potential, and therefore the sorption isotherm for the sample can be recalculated from the known sorption isotherm of the reference solid. The range of pores covered depends on the reference pore size distribution. Using several reference materials (RMs), it is possible to measure sorption isotherms in the range of capillary pressures 10^7 N·m^{-2} to 10^3 N·m^{-2}, which corresponds to the range of the pore sizes 10^{-2} to 10^2 µm.

Liquid and contact porosimetry techniques cover the range of pore size spanning several decades, thus allowing for the assessment of the fractal properties of porous materials of hierarchical structure. Neimark [22,23] developed the thermodynamic method for calculating the fractal dimension from adsorption and capillary isotherms. Contact porosimetry [24] was used for characterizing the pore structure of peat in the range of pore width from 1 to 1000 nm.

4.3 Capillary condensation and evaporation in the macropore range

4.3.1 Principle, interest, and difficulty

Mesoporous materials are routinely characterized by adsorption–desorption from the gas phase in the pressure range associated with the phenomenon of capillary condensation, which is generally accompanied by a hysteresis loop in the adsorption–desorption isotherm. The mesopore size distribution (i.e., in the range 2–50 nm) is derived either by the application of procedures based on the Kelvin equation, such as the Barrett–Joyner–Halenda (BJH) method, or more recently by the application of density functional theory (DFT).

The same approach is applied here in the macropore range where, theoretically, the Kelvin equation should be less questionable than for mesopores, since it is based on a classical macroscopic thermodynamic approach, which is more strictly applicable to interfaces of low curvature. Conversely, the practical requirements involved in controlling capillary condensation in the macropore range are very demanding. The main difficulty is that for large accessible pores with sizes above 50 nm, capillary condensation occurs at pressures very close to the saturation pressure of the adsorptive. For example, in the case of nitrogen, if the maximum relative pressure reliably measurable is 0.99, the maximum equivalent pore diameter is only around 200 nm, as calculated by the Kelvin equation.

4.3.2 The bulk condensation method

In order to extend the capillary condensation range as far as possible to provide a reliable Kelvin or DFT analysis, the "bulk condensation method" has been proposed [25]. The procedure involves analysis of the desorption isotherm after "oversaturation" of the sample to be sure that all the pores have been filled. This simple procedure allows the range to be extended up to ca. 400 nm with conventional nitrogen adsorption apparatus [26].

To reach larger pore widths, it is necessary to overcome various technical difficulties, notably by minimising temperature gradients in the experimental system. The major difficulty with a standard apparatus is that there is inadequate temperature control when working close to the saturation pressure. Condensation can then occur at any cold point of the adsorption cell, prior to taking place in the sample itself.

4.3.3 Water desorption calorimetry

This problem was solved in part by Denoyel et al. [27], who set up a desorption experiment that takes advantage of two features of a Tian–Calvet diathermal calorimeter, namely, (i) its ability to monitor closely from the heat exchanged the amount of adsorptive condensed or vaporized and (ii) its exceptional thermal stability (within 10^{-5} K over many hours for the difference in temperature between sample and reference cell). The principle of the set up is shown in Fig. 2. The porous sample is saturated with a liquid that is slowly desorbed in quasi-equilibrium conditions. The equilibrium relative pressure is deduced from a differential transducer between the sample cell and the reference cell that is filled with pure liquid (e.g., water). The heat flow is used to determine the amount of desorbed liquid.

Despite a few problems still to be resolved, this method allows the determination of pore size up to around 10 μm. Since it is based on the corrected Kelvin analysis, the multilayer vs. pressure relation must also be known over the range of high relative pressure. By using liquids with various values of surface tension, it should be possible to study the wettability and the hydrophilic character of a macroporous material.
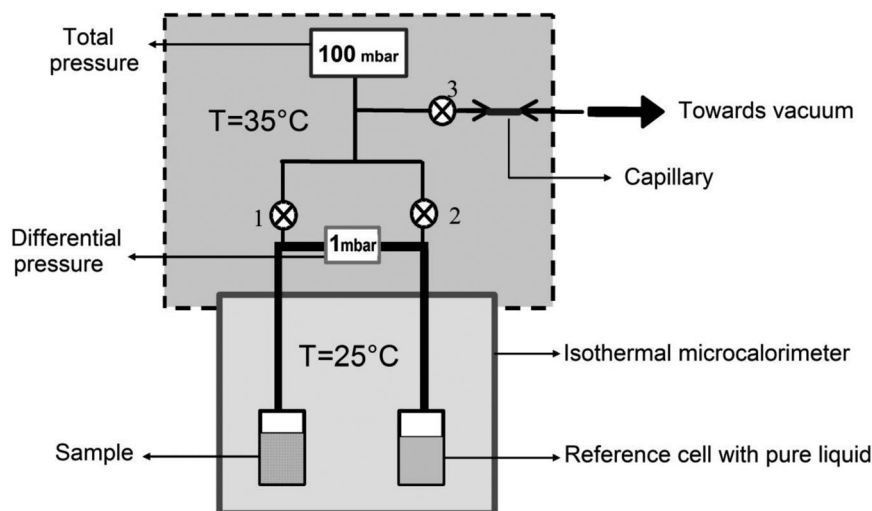
Fig. 2 Principle of a set-up for water-desorption calorimetry.

5. PERMEATION OF A LIQUID

Porous materials can be characterized by the permeation of a gas or a liquid. Many applications of porous materials involve the flow of gas or liquid through the material and the ability to predict or at least correlate the pressure drop with the flow rate is essential. With the aid of an adequate model, the assessment of pore size is possible. For the laminar flow regime, permeation through a porous material is described by Darcy's law:

$$u_{sf} = \frac{\kappa}{\eta} \frac{\Delta p}{L} \tag{2}$$

where u_{sf} is the superficial fluid velocity (normally expressed in m·s^{-1}), η is the fluid viscosity (in Pa·s), Δp is the pressure drop (in Pa) over a layer of thickness L (in m) of material, and the permeability is κ (in m^2). This equation holds for the laminar or viscous flow regimes. Extension to the turbulent flow regime is possible, where inertial forces dominate, but seldom applied to permeability measurements. Thus, the flow and pressure drop are usually measured over a wide enough range to ensure linearity and laminar flow.

To link the permeability to pore size or other characteristics of the material, a model is needed for structure or texture. When the structure is not exactly known or difficult to describe, the flow of a liquid through a porous material can still be described by the Hagen–Poiseuille or Kozeny–Carman equation.

The *Hagen–Poiseuille* equation is based on the assumption of *parallel uniform cylindrical pores* of diameter d_H

$$\frac{\Delta p}{L} = \frac{32\eta u_{sf}}{\varepsilon d_H^2} \tag{3}$$

where ε is the porosity accessible to flow (e.g., external porosity of packed bed). For noncylindrical pores, the hydraulic diameter can be used (flow area divided by wetted perimeter). One can correct this equation for tortuosity of the pores if known by correcting the length L by the tortuosity factor τ with allowance for a longer flow path. Formulas somewhat deviating from eq. 3 are used to extract the pore size, e.g., for monolithic chromatography packings [28]:

$$d_{\mathrm{H}} = 2 \left(\frac{5\kappa}{\varepsilon} \right)^{1/2} \tag{4}$$

The *Kozeny–Carman* equation [29] assumes the pores to be voids between *closely packed spheres* of equal size d_{p}, using the concept of hydraulic radius to obtain the equivalent cylindrical pore diameter

$$\frac{\Delta P}{L} = \frac{180\eta(1-\varepsilon)^2}{\varepsilon^3} \frac{u_{\mathrm{sf}}}{d_{\mathrm{p}}^2} \tag{5}$$

which is valid in the laminar regime or for small-particle Reynolds numbers below 1:

$$\mathrm{Re}_{\mathrm{p}} = \frac{u_{\mathrm{sf}} d_{\mathrm{p}} \rho}{\eta(1-\varepsilon)} \tag{6}$$

with ρ the fluid density (kg·m^{-3})

Somewhat more generally, one can calculate the permeability in this Kozeny–Carman model as:

$$\frac{\Delta P}{L} = KS^2 \frac{(1-\varepsilon)^2}{\varepsilon^3} \eta u_{\mathrm{sf}} \tag{7}$$

where K is the Kozeny–Carman factor estimated (or assumed) to be 5 as in eq. 5 for closely packed spherical monodispersed particles with tortuosity factor $\tau = 2.5$, and S the particle-specific surface area (in m^2·g^{-1}) derived from $S = 6/\rho_{\mathrm{p}} d_{\mathrm{p}}$ (with ρ_{p}, the absolute density of the particles and d_{p}, their diameter in μm). An extension of the porosity function obtained for this model to porous materials with an interstitial porosity much higher than that of a random close sphere packing or to different types of material is physically not consistent and will therefore lack accuracy. Strong deviations of K from the value of 5 have been found with values as low as 2 and above 100 (with porosities greater than 0.9).

The Kozeny–Carman and Hagen–Poiseuille equations do not fit the experimental data, and hence do not give a reliable particle or pore size, when the texture of the porous material exhibits at least one of the following characteristics:

- high porosity, significantly deviating from the 0.4 for packed spheres (say above 0.7),
- particles very far from spherical shape (flaky materials, fibres),
- consolidated porous media (of compressed deformable particles), or
- multimodal or very large grain or pore size distribution.

The range of validity of the Kozeny–Carman equation can be extended to porous materials having the above-mentioned characteristics as long as the effective values of the texture parameters ε, d_{p}, and τ for these types of media can be determined experimentally, and this deviation is incorporated in an adequate model [30,31]. As an example, using the standard Kozeny–Carman analysis with $K = 5$, an equivalent spherical particle size of 15 μm is found for a chromatographic silica monolith with 1.9 μm pore size [32].

A major problem with the method is that when a material is composed of *pores with different pore sizes*, and considering that the flow rate through the larger pores will be more than proportionally larger than the flow through the smaller pores [flow rate ~ (pore diameter)[4]] it is to be expected that the observed flow resistance in the case of a distribution of pore sizes will always be smaller than the flow resistance calculated on the basis of the average pore size. Hence, *the estimated pore size will always be large* compared to other methods. The method is able to predict the difference in flow or pressure drop, certainly in comparing the behaviour of particle beds or monoliths in chromatography, but may not yield the correct pore dimensions in relation to other phenomena such as diffusion [33]. Recently,

attempts have been made to find the appropriate length scale in a porous structure to insert in the Kozeny–Carman equation [34–36].

Although the principle of the permeation measurement is fairly straightforward, it is not a trivial task to perform a reproducible and accurate determination, and no standard equipment is readily available with broad applicability. Basically, one has to either generate a flow and measure the resulting pressure drop, or apply a differential pressure and measure the resulting flow. Either a gas or a liquid can be used, but in the case of the gas one has to ensure that the flow is by viscous forces and not by diffusion, which may be dominant for very small pores [37]. Some of the issues involved are mainly linked to sample preparation and finding an adequate flow and pressure measurement window. A sample through which one wants to measure flow should be cut (often in cylindrical form) from the material and fitted in a tube, avoiding at all cost leaks between sample and wall. Usually the sample will be glued in place with epoxy glue or fine inorganic cement, which should not penetrate appreciably into the material and disturb the flow pattern. The sample diameter should be large enough across the flow direction to be representative and avoid wall effects owing to porosity changes close to the wall, usually extending more than 5 particle diameters from the wall (preferably 20 to 100 times the largest flow pore or channel). Sample length can be adjusted to adapt to available flow and pressure measurement. Before starting a measurement, the material should be evacuated to allow full penetration of the liquid and avoid dead zones where air is trapped. Obviously, an inert wetting liquid should be used properly degassed. Liquid syringe pumps and liquid chromatography pumps are often suitable for such measurements as they can cover a wide pressure range up to several 10.0 MPa. Provided one can measure low flow rates (e.g., by collecting the liquid and measuring it gravimetrically), differential pressure can be reduced to avoid material damage or compression, especially a problem with soft compressible or fragile materials. Sample size can range from a fraction of a gram or millilitre to large blocks of the material. Smaller samples are obviously more difficult to machine or form in the right shape and mount for the flow experiment. Materials with fine pores exhibit very low flow rates for reasonable pressures.

The experiment can be arranged so as to have either horizontal or vertical flow through the sample. Great care must be taken in every case to prevent bypassing of the sample by the liquid (see Fig. 3). It should be taken into account that some liquids might change the pore structure and therefore the permeability, owing to the rearrangement of some particles, swelling of certain materials, chemical reactions, etc.
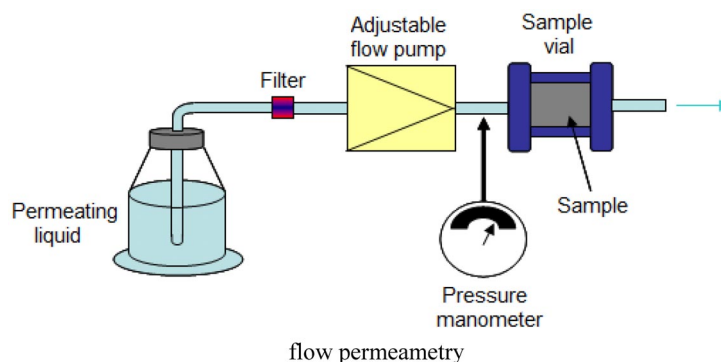

flow permeametry

Fig. 3 Principle of liquid-flow permeametry.

To conclude, the measurement of permeability is a simple and fast method for the estimation of the pore hydraulic radius, but certain precautions are required. Among them, the most appropriate theoretical approach should be chosen, together with a non-wetting liquid, and the influence of the pore

geometry and tortuosity on the interpretation of the results should be considered [38]. This method is applicable in the 0.1 to 1000 µm range.

6. FREEZING–MELTING POROSIMETRY

6.1 Principle of the method

When a liquid fills a porous medium, confinement changes its properties: in particular, its freezing point is most often depressed, along with the subsequent melting point. These temperature depressions are dependent on the *pore width*, but to derive the pore size distribution one also needs to assess the corresponding change in volume of the liquid phase (i.e., the *volume of pores of a given width*). As will be seen hereafter, this is currently done with help of either differential scanning calorimetry (DSC) or NMR.

A careful thermodynamic analysis of the method, in its DSC version, was carried out by Brun, Quinson, and Eyraud [39].

Because the effects of confinement are much easier to detect in mesopores than in macropores, most measurements by freezing–melting porosimetry have been carried out on mesoporous solids. Also, since the method does not hold for microporous solids (where real freezing does not take place) it can be considered to cover a similar range to that of the BJH adsorption–desorption method. However, as in the case of capillary condensation, as will be seen, various recent attempts have been made to extend its application to the macropore range.

6.2 Version based on DSC: "Thermoporometry"

In this version, the total change in energy associated with the freezing–melting process is monitored by following the heat produced or absorbed by the sample. Thus, the heat released at a given temperature is proportional to the amount of phase-changing component. Therefore, the size and temperature location of the DSC peaks observed during the melting or solidification of the confined fluid are directly related to the pore width distribution. The basic equation used in thermoporometry (and which is analogous to the Kelvin equation for capillary condensation) is:

$$\frac{1}{r_p - t} = -\frac{1}{2\gamma_{sl}} \int_{T^\circ}^{T} \frac{\Delta_m H}{v_l T} \, dT \tag{8}$$

where r_p is the pore radius in which the solidification occurs at temperature T (T° is the bulk solidification temperature), γ_{sl} the solid–liquid surface tension (i.e., ice water), $\Delta_m H$ the melting enthalpy, v_l the molar volume of the fluid, and t the thickness of the bound layer (assumed to be constant and independent of T). This bound layer corresponds to a film of adsorbed water that does not undergo any phase change in the considered temperature range. This is due to an extra-depression of the freezing temperature, which results from the proximity of the surface. The pore size distribution is derived directly from the DSC recording of the calorimetric peak by the following equation:

$$\frac{dV}{dr_p} = k \frac{(\Delta T)^2}{Q} y \tag{9}$$

where y is the heat flow measured by DSC and k is a constant related to the temperature scanning rate and to the parameters of the equations $r_p = f(T)$ derived from eq. 8, and where Q is the heat measured and also the enthalpy of melting. For a macroporous sample, the experiment requires a slower heating rate than for a mesoporous one and will take ca. 3 h.

The method has its limitations: for instance, in the same way that mercury intrusion porosimetry (MIP) requires an assumed value for the contact angle, here an assumption must be made for the solid–liquid interfacial tension, which is not directly measurable (unlike the liquid–vapour interfacial tension). Also, the melting (or freezing) enthalpy depends on the temperature at which the phase change takes place, and this is also not directly measurable. Calibrations are therefore required. However, the parameters already determined by Brun et al. [39] are available in the case of water. In Fig. 4, an example of DSC recording is given for a macroporous controlled pore glass, while the corresponding cumulative pore size distribution is shown in Fig. 5 together with that obtained by mercury porosimetry and by water desorption calorimetry (after Barrande et al. [40]).

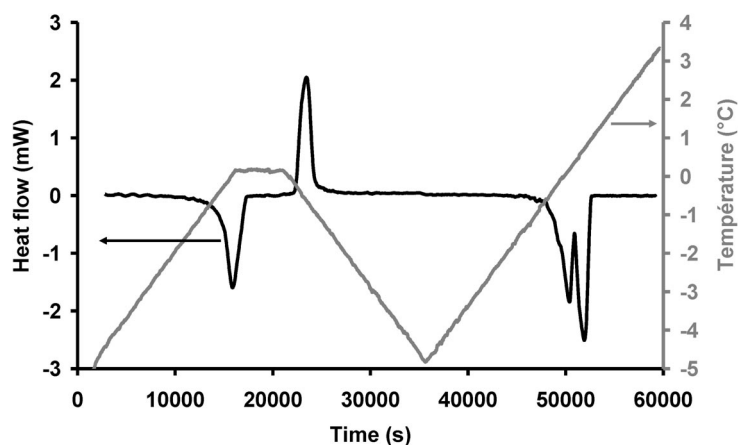

Fig. 4 DSC trace of a thermoporometry experiment (water in macroporous porous glass).
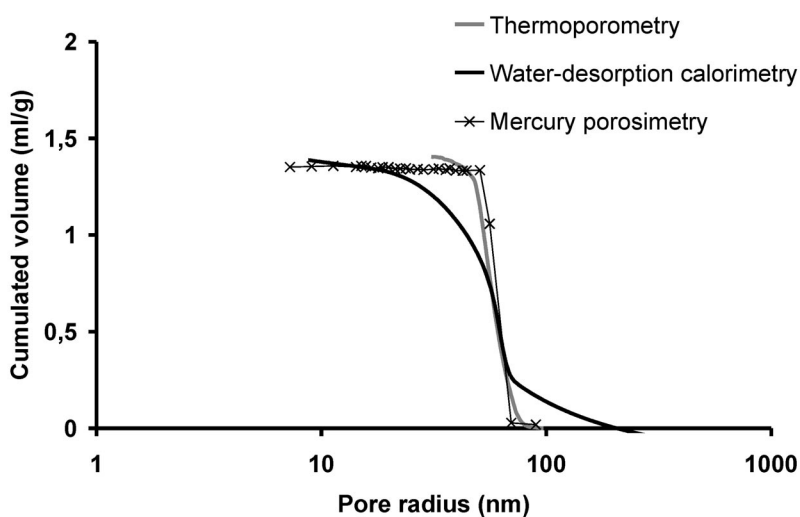

Fig. 5 Pore size distributions determined by thermoporometry, water desorption calorimetry, and MIP for a controlled macroporous glass (after [40]).

6.3 Version based on nuclear magnetic resonance: "NMR cryoporometry"

This is another promising approach [41], which is of particular interest when standard NMR equipment is already available. Basically, the melting point distribution is now determined by analyzing the change in the proton NMR signal as a function of temperature. More precisely, the volume of liquid (pore volume) that appears progressively when increasing the temperature is measured quantitatively, after the amplitude of the NMR signal, with a spin-echo method that discriminates clearly between the liquid and solid NMR contributions. The melting temperature $T_m(x)$ of the embedded liquid is related to the pore size distribution by

$$\frac{\mathrm{d}v(x)}{\mathrm{d}x} = \frac{\mathrm{d}v(x)}{\mathrm{d}T_m(x)}\frac{\mathrm{d}T_m(x)}{\mathrm{d}x} = \frac{\mathrm{d}v(x)}{\mathrm{d}T_m(x)}\frac{k}{x^2} \tag{10}$$

where v stands for the frequency shift and x for the pore size, and where k is a constant only depending on the liquid used (water, cyclohexane…).

Examples of application of the technique are given in Figs. 6 and 7 for cyclohexane in a controlled mesoporous silica glass of 20 nm diameter. In Fig. 7, the comparison with nitrogen adsorption–desorption measurements is also given. The measurements are reproducible and fairly rapid (2 h for a mesoporous sample, with determination on a proton NMR spectrometer at 14.3 MHz). As in thermoporometry, more time is required with a macroporous sample, since the heating or cooling rate must be lower. Cyclohexane is a particularly favourable liquid to use because it has a large melting point variation with pore size and forms a plastic crystalline phase below its melting point, which does not appear to damage any delicate pore structure.

Recently, NMR cryoporometry has been applied to the macropore range [42]. By using octamethylcyclotetrasiloxane as a probe liquid, it seems possible to study the pore size range from 10 nm up to 1 µm.
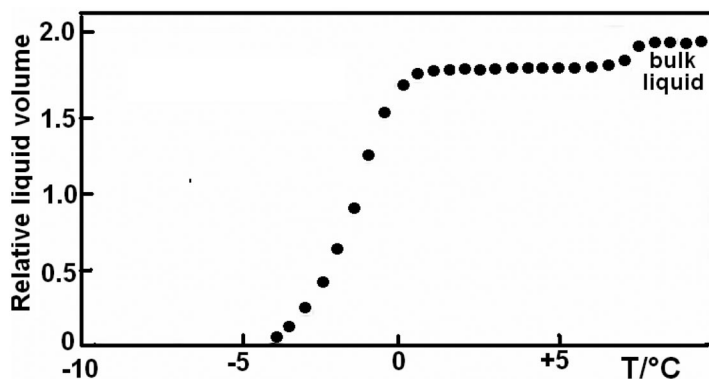

Fig. 6 Volume of molten cyclohexane (arbitrary scale) vs. temperature, as determined by NMR cryoporometry, for Sorbsil silica.
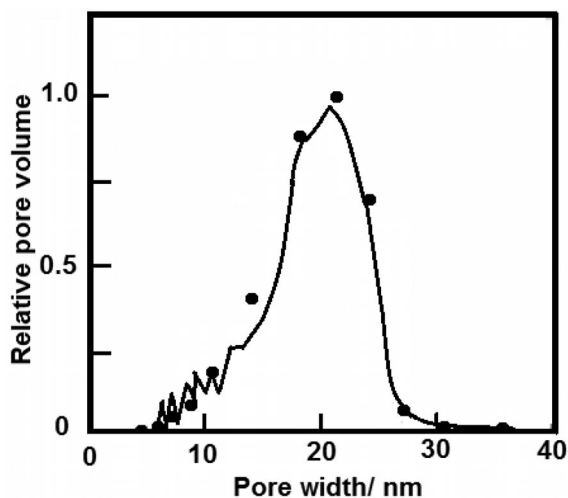
Fig. 7 Pore size distribution of silica, as determined by NMR cryoporometry using cyclohexane. Dots show results from BJH analysis of N_2 adsorption–desorption isotherm.

6.4 Merits and limits of freezing–melting porosimetry

An attractive aspect of freezing–melting porosimetry is that it can be used in laboratories that are not equipped with gas adsorption or mercury intrusion equipment, but that have analytical DSC or NMR facilities. Also, it is the appropriate method for the study of wet or fragile samples such as hydrogels or living materials, which undergo changes when the liquid phase is removed. Moreover, it has the advantage of being a relatively fast "clean" method—generally with water used as the freezing–melting liquid. A pore size distribution determination can typically be completed within ca. 3 h in comparison with nitrogen adsorption–desorption, which may take up to 24 h!

Of course, the sample must be able to withstand contact with liquid (water or an organic) without undergoing any unwanted transformation. As with any other method, it must be assumed that all the pores in the sample are rigid with the same standard shape (e.g., cylinders or slits). Calibration is required with reference porous materials, ideally of pore size and chemical nature comparable to the sample.

The critical factor for the method to be applied in the macropore range is the temperature control. This is illustrated by the DSC results in Fig. 4 where the melting peak of water in pores is not fully separated from that of water outside particles. Although the resolution of the temperature determination is very high in a DSC measurement, to achieve both selectivity (in pore size) and sensitivity (in pore volume) requires a compromise between the scanning speed, the response time, and the baseline quality of the calorimeter. For NMR, the limitation is also in the temperature control. For example, the assessment of a pore width of ~1 μm requires the detection of ~0.1 K depression from the bulk freezing point.

7. IMAGING TECHNIQUES

A number of methods allow the imaging of macroporosity within a solid. All of them are based on the interaction of an electro-magnetic, magnetic, or electronic radiation with the solid containing voids.

7.1 Magnetic resonance imaging (MRI) [43]

MRI generally requires the use of a probe fluid within the void space because the NMR line widths for most solids are so broad. Typical MRI studies of porous solids will involve ^{1}H NMR of suitably wet-

ting probe fluids, such as water or hydrocarbons. Positional information is encoded into the NMR signal by means of field gradients, since the Larmor precession frequency is a function of field strength. MRI can characterise the void space directly, if the pores are sufficiently large, or indirectly, using contrast techniques for smaller pores. The resolution limit for direct visualisation is ~10 μm. For macropores below the resolution limit, NMR contrast methods, such as relaxation time or pulsed-field gradient (PFG) techniques (see also Section 7.5), are combined with the basic imaging experiment to provide spatially resolved maps of the local average porosity, pore size, and network tortuosity for pore sizes down to the mesopore range. The lower detection limit is determined by the very short relaxation time of the smallest pores. The resolution limit for indirect visualisation is generally controlled by the root mean square (rms) displacement of the probe fluid during the experiment, as this potentially blurs the image.

Pore size mapping, using relaxation time contrast techniques, are only really appropriate for use with chemically homogeneous materials, such as relatively pure silica and alumina catalyst supports, and would generally be unsuitable materials with substantial concentrations of paramagnetic species, or for partially coked heterogeneous catalysts. This is because NMR relaxation of pore fluids would be affected by, for example, heterogeneous distributions of paramagnetics, as well as pore size variation.

7.2 (Computerised) X-ray tomography (CXT)

CXT for characterising porous media is similar to that used for medical purposes. Micro-CXT consists of passing X-rays through an object along many different paths in many directions. The object under study is rotated inside the X-ray chamber so as to be viewed from different angles. A computer records each of the projected images and measures the intensity of the X-ray beam after it passes through the material. The sample is then rotated by a small angle, and the process repeated. Once the initial data are obtained, image reconstruction is accomplished via a filtered back-projection algorithm utilising cone-beam reconstruction. The reconstruction results in a set of 2D cross-sectional images, or slices, for the entire sample, which thereby reveals the internal microstructure of the sample. Spatial resolution is possible down to ~100 nm for synchrotron radiation sources, and ~100 nm to 1 μm for desktop apparatus [44]. Hence, large macropores may be imaged directly. For materials with pores of size less than the resolution limit, the spatial variation in porosity can be imaged by filling the void space with a suitable contrast agent such as di-iodomethane, or mercury, as done to prepare the images shown in Fig. 8. Di-iodomethane is of course preferable from the environmental viewpoint, but use of mercury porosimetry permits selective visualisation of particular pore size ranges (see Section 7.6). A comparison of the X-ray absorbance against a suitable set of standards enables the voidage fraction in each image voxel (i.e., volumetric pixel) to be evaluated; CXT can also be made element specific using so-called K-edge imaging [45].

High electron density differences within a sample can lead to scattering of the X-ray beam, and to artifacts within the image. The size of the sample that may be studied is limited by the penetrating power of the X-ray beam, and can also lead to image artefacts. The sample thickness should typically be in the millimetre to centimetre range.
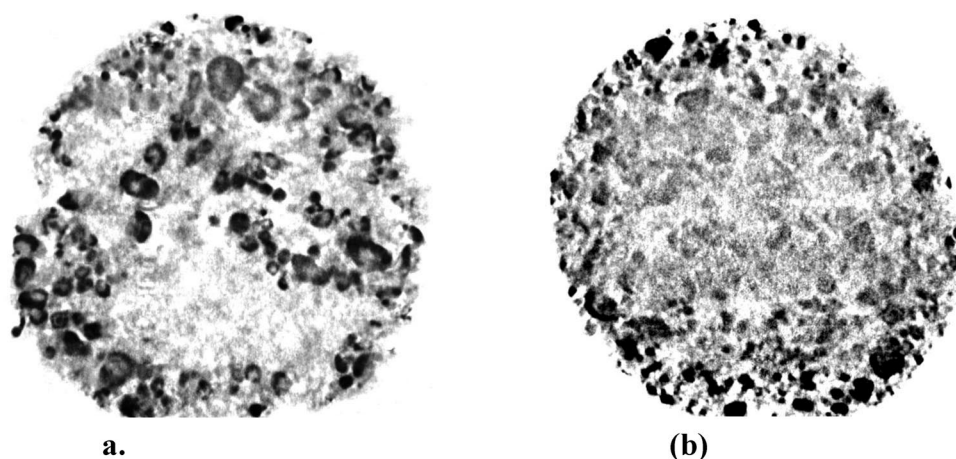
Fig. 8 CXT images of cross-sections through a macroporous alumina pellet following mercury porosimetry scanning loops up to (a) 0.22 MPa and (b) 0.54 MPa. The typical pellet diameter was ~4.5 mm. The black and dark regions correspond to entrapped mercury, while the light grey regions correspond to alumina matrix. Mercury percolation pathways through the pellet can be discerned (with kind permission of Taghi Miri and Serafim Bakalis, University of Birmingham, UK).

7.3 Electron microscopy (EM)

Two EM methods are suited for examining macroporous materials.

Electron tomography, also known as 3D-TEM [46], is based on similar physical principles as CXT, except that the penetrating radiation is a beam of electrons, rather than X-rays. The spatial resolution possible with 3D-TEM is of the order of a few nanometres. However, the resolution is limited by sample size (e.g., <~500 nm for ~1 nm resolution) and the angle through which the sample stage may be turned. A particular problem with 3D-TEM is the possibility of image artifacts owing to sample ablation from the electron beam.

Dual-beam EM methods [47] have the same underlying physical principles as microtoming for light microscopy. The technique employs two particle beams, first, a focused ion beam (FIB), usually gallium ions, to ablate the surface of the sample to reveal one layer at a time, and, second, the electron beam to obtain the image. If a series of images is obtained of successive layers of a sample then these can be reconstructed into a full 3D representation of the void space. Nanoscale resolution may be achieved.

Both of the above EM methods suffer from the drawback that, to achieve nanoscale resolution of the void space, the sample size itself must also be very small. Hence, to obtain a statistically representative sampling of the void space of materials with significant macroscopic (>10 μm) heterogeneities in the spatial distribution of pore space characteristics, such as those observed by MRI [43], truly astronomical numbers of samples need to be studied.

7.4 Light microscopy/laser methods

The confocal laser scanning microscope (CLSM) [48] is based on the principle that optics reject light from outside the focal plane such that the resulting image is a true optical section, and this capability allows imaging at different depths inside translucent samples. More opaque samples can be imaged if they are sliced into sections that are themselves translucent. The slice thickness can be as thin as ~0.5 to 1.5 μm, but is dependent upon the numerical aperture of the objective lens. At present, these methods allow the assessment of pore sizes above ~1 μm.

7.5 Pulsed-field gradient (or pulsed-gradient spin-echo, PGSE) NMR

PFG NMR [49] enables the straight-line path displacement of fluid molecules undergoing self-diffusion within a void space to be determined. The technique is based on the use of magnetic field gradients to detect motion. Initially a molecule is labeled with its starting position, then allowed to diffuse, and its new position is then determined. Depending on the relative sizes of the length scales of the molecular displacement, and the pores within the porous medium, a range of void space parameters can be determined. The typical rms displacement of a liquid, such as water, during the course of the experiment is ~10 to 100 µm. For void spaces with individual pores much smaller than the rms displacement, then the tortuosity of the pore network can be determined. If the rms displacement is of the order of the size of the pores, then the surface area-to-volume ratio of the pores can be determined. PFG NMR allows the assessment of pore sizes of ~10 µm or greater.

7.6 Hybrid imaging and other methods

Imaging techniques of various modalities can be fully integrated with other more indirect methods, such as non-wetting liquid intrusion, to obtain more information concerning a particular porous structure than is possible using either technique alone, or simply combining the data from separate experiments. For example, CXT has been used in conjunction with low melting point alloy intrusion [50], or mercury porosimetry [51], to obtain more information on the pore structure of macroporous materials with pores too small to be imaged directly. MRI has been used to obtain pore structural models with which to interpret indirect methods, such as mercury porosimetry [51], which remove some of the plethora of freely adjustable model parameters possible when interpreting porosimetry data using network models. In a bidisperse alumina material, where integrated gas sorption experiments revealed that mercury entrapment occurred only within macropores of a size ~1 µm [52], CXT was able to reveal the heterogeneous spatial distribution of these macropores despite the fact they were too small, and interspersed with mesopores, to be observed individually using MRI, or desktop CXT alone. CXT images of entrapped mercury following porosimetry can be used [51] to validate physical models of mercury retraction for a given disordered material, which can then be used to interpret retraction curves to obtain information on the spatial distribution of pores for materials not amenable to MRI techniques.

8. STATISTICAL RECONSTRUCTION OF POROUS MATERIALS

8.1 Introduction

The methods used to assess macropore size distributions and described in the previous sections of this document are all based on simple representations of the porous medium, with a single pore shape: cylindrical, slit-shaped, or voids between close-packed solid spheres. A more refined use of the experimental data necessarily raises the challenge of describing the geometry of the pore network.

For disordered materials, it becomes evident that porous media must be characterized in statistical terms [53,54]. Here, direct 2D and 3D observations can be used through an imaging protocol followed by an image analysis. In parallel, mathematical pore models or the statistical reconstruction are useful "toy models", allowing the classification of the media and providing a better understanding of the relation between geometry, transport, and thermodynamics processes and mechanical behaviour [55,56].

In addition, the statistical modelling approach can be adapted to provide an improved understanding of the phenomena involved in methods of characterisation (such as adsorption, capillary condensation, permeation, molecular diffusion, excitation relaxation, or phase transitions…).

8.2 Toolbox for modeling

Since our aim is to discuss and to analyse forms, shapes, and patterns, it is useful to recall some morphological tools. At present, it is difficult to provide 3D representations of many porous media using conventional or even more sophisticated 3D imaging techniques. It is more convenient to work on 2D sections of the material. Among all possible metric parameters, it is of interest to identify those global parameters, which can be estimated in either 2D or 3D. This is the aim of stereology [57]. These parameters have to satisfy a number of criteria, the so-called Hadwiger conditions [57]: (1) they have to be invariant by translation or by rotation of the material; (2) they have to satisfy the homogeneity conditions; (3) they have to be continuous functions; (4) and they have to satisfy the additivity conditions. Under such constraints, four functionals (also called Minkowski functionals) can be defined: the porosity, the specific surface area, the integral of mean curvature, and the integral of Gaussian curvature [58]: The first three can be measured on 2D sections while the last one, related to the topology of the pore network, can only be estimated on 3D representations. Recently, a new attempt has been made to characterise irregular spatial structures by parallel sets and these four integral geometric measures [59].

Several variant strategies provide a metric characterisation in terms of the probability density function. This is a more detailed approach allowing a closer inspection of the geometrical features. In the following, we will mention two of them, the local porosity distribution and the chord length distribution functions.

The local porosity distributions were originally introduced as a quantitative substitute for pore size distributions [60,61]. The idea is to measure porosity or other well-defined geometric observable distribution within a 3D box having a size L. This box is uniformly distributed in space in order to fill the pore network field of view. The evolution of the porosity histogram with L reveals a progressive passage from a local picture where a trivial bimodal distribution (0,1) is observed to a macroscopic average picture associated with a peak around the macroscopic porosity value. Such a histogram evolution is a good tool to analyze any possible existence of a representative elementary volume (REV). This strategy can also be extended to analyze the connectivity fluctuations using local percolation probability [62].

The chord distribution functions [63,64] provide a complementary way to get a more complete stereological analysis of a porous material. These functions can be computed either in 2D or 3D assuming some general conditions similar to the Hadwiger conditions. Their determination helps us to clarify some questions about average pore size, mean curvature, pore shape, surface roughness, and structural correlation between points belonging to the solid, the interface, or the pore network. A chord is a segment belonging either to the pore network (p) or to the solid matrix (m) and having its two extremities on the interface. There are several ways to define chord length distribution functions depending on the chosen angular average. In the following, we use the classification introduced by Colemam [65] and discuss mainly the μ-chord properties. μ-Chords are obtained by tracing random and homogeneously distributed straight lines (rays) through a section or a 3D structure. The chord length distribution function gives the probability of having a chord length between r and $(r + dr)$ belonging either to the pore network [$f_p(r)$] or to the solid matrix [$f_m(r)$]. The μ-chord distribution functions can either be computed inside a 3D structure or through a random section of the pore network. In both cases, the final results will be similar, assuming some general properties such as a statistical isotropy. The two first Minkowski functionals, namely, Φ and Sv, are directly related to the first moments of $f_p(r)$ and $f_m(r)$. Chord distribution functions are sensitive to the type of structural disorder. This point is discussed elsewhere [63] and allows us to consider μ-chord distribution functions as fingerprints of the local and semi-local morphology of the pore network.

An alternative way to probe the pore network morphology is to look at structural correlation [66]. The goal is to correlate the structural state (i.e., with reference to the solid matrix or to the internal interface) of two distinct points separated by a distance r. These structural correlations quantify how the "memory" of an initial state is progressively lost when a point is moved away. Two point correlation

functions such as the bulk, the surface autocorrelation, or the pore surface correlation functions can be defined. They play a central role in different processes involving energy, excitation, or molecular transport. Moreover, as shown in the seminal work of Doi [67], these three correlation functions are directly involved in an upper bound limit of the permeability. Clearly, a statistical geometrical analysis of these two point correlation functions is required. It is of interest to define the so-called REV size, above which the disordered structure reaches a homogeneous distribution. However, some caution should be exercised concerning the way used to estimate the appearance of a two-point correlation function plateau at large distance. Interestingly, 3D structural correlations can be experimentally probed, using small-angle X-ray or neutron scattering (SAXS, SANS) [68].

An important question concerns the connectivity of the pore network (or the solid matrix) at different length scales. A geometrical set X is interconnected when every pair of points belonging to X may be joined by a curve included in X. Clearly, the connectivity is an important characteristic for transport properties such as molecular diffusion or fluid permeability. The pore network is essentially defined by its internal interface. The topology, mainly the connectivity, is related to the genus G of this interface [69]. The genus of a surface is the maximum number of ways a surface may be cut by closed loops without losing its initial connectivity. $G = 0$ for a sphere, and $G = 1$ for a torus. The genus is not additive, and it is necessary to introduce another topological parameter, the Euler Poincaré constant N_3 of the pore network [57,69]. The N_3 is additive and is directly related to Gaussian curvature properties of the internal interface. In the case of a collection of disconnected particles, N_3 is exactly the number of objects. For a pore network delimited by a unique multiconnected interface having a genus G, N_3 is equal to $1 - G$.

A powerful tool to describe the topological architecture of porous media is the linear graph of retraction [69–71]. This graph is obtained by progressively narrowing the pore space starting from the internal surface. This "thinning skeletizing" must satisfy both topological (invariance of the three first Betty numbers [69]) and geometrical constraints in order to fit as exactly as possible the "skeleton graph". A difficult step is to reduce the numerical skeleton in terms of a simple graph made of vertices connected by edges and having the same topological properties. One ends up with a simple 3D map of the pore network. The knowledge of the pore network and the linear graph of retraction opens up the possibility of defining and extracting "elementary pores" and analyzing the statistical morphology in relation with transport [72] or mechanical properties [73].

8.3 Some ways of modeling disordered porous media

One approach is to *simulate or mimic the physical and chemical processes involved in the formation* and development of the pore structure. This approach has to be made on a case-by-case basis and requires a preliminary understanding of the basic principles and mechanisms of the synthesis of the porous material. Moreover, the finite size of simulated systems is a serious technical difficulty, especially when the simulation is performed on the atomic scale. In these conditions, it is generally difficult to sample long-range connectivity and large REVs.

An alternative strategy for modeling is to perform the *reconstruction of the porous structure from* limited but relatively accurate *structural information about the porous material under study*, but this "inverse problem" has no general or exact solution.

8.3.1 Random models from mathematical morphology [57,74]
Extended development of mathematical morphology has generated various classes of random closed sets. For each of them, the constructive protocol is well defined and several geometrical properties can be analytically demonstrated. These sets serve as general mathematical models for irregular geometrical patterns and can be used to mimic porous disordered media. In the literature, various mathematical models are proposed such as Boolean, dead leaves models, Poisson tessellation and Poisson processes, and also Voronoi tessellation. Of particular interest is the percolation transition and the associated geo-

metrical representation of the pore network on- and off-lattice [56–83]. This model is also a form of "wild representation" exhibiting statistical scale invariance. In all cases, one essential point is to experimentally confirm that the chosen generic model captures some key structural properties of the real pore network under investigation.

8.3.2 Constrained models from experiment

8.3.2.1 3D reconstruction using correlated Gaussian fields [75–77]
By starting from the knowledge of bulk autocorrelation function of the matrix, it is possible to rebuild a 3D pore network having the same characteristics (mainly having a similar specific surface area, pore volume, and bulk–bulk correlation function). Such reconstruction is based on the use of correlated Gaussian fields. Critical evaluation of these reconstructions and comparison with experiments can be found in the literature [77]. These models succeed in generating realistic representations of long-range Debye disorder, mass or surface fractals, and some correlated bicontinuous media (e.g., Vycor glass, sponge phase, bi-continuous emulsions). A challenging problem is to be able to impose, during the 3D reconstruction, some constraints on the generic shape of the interface in order to mimic, for example, a disordered granular solid made of spherical and/or ellipsoidal particles.

8.3.2.2 3D reconstruction using simulated annealing [78–81]
The former strategy based on Gaussian random fields gives successful reconstructions of many classes of nonparticulate composite materials. However, with several systems such as granular materials, additional morphological information is required. It is then necessary to go beyond the two-point correlation function and add other types of correlation functions in order to get a more constrained reconstruction procedure. Several authors have recently proposed another stochastic reconstruction technique based on a simulated annealing method. Using either a 2D section of the material or information from small-angle scattering, it is possible to derive 3D reconstructions of particle suspensions, colloidal pastes, and porous rocks. Various experimental constraints can be selected (2 points correlation function, chord length distribution functions, tortuosity, etc.) to generate a numerical toy model. One difficulty during generation of an extended configuration of the pore network is the long computational time needed to converge. Some recent strategies have been proposed to improve such a situation.

8.4 The fractal approach: A model for a wild disorder at all scales [82,83]

The degree of disorder is another way of classifying pore textures. Many porous media are relatively homogeneous above a defined length scale. It is then easy to find the REV, which is meaningful above the particular length scale. This type of matrix could be called a "weakly disordered texture". On the other hand, numerous materials exhibit hierarchical organization with strong disorder and heterogeneity at different length scales. In this case, an appropriate REV cannot be defined, and any averaging is length-scale-sensitive. Fractal geometric [56,82] description provides a simple way to go from one to another length scale. The associated geometrical transformation is based on statistical length scale invariance. A fractal object keeps the same statistical morphology on a magnification or a change of scale. Fractal structures are encountered in numerous natural porous structures. These structures are often generated during an out-equilibrium morphogenesis such as precipitation, irreversible aggregation, dissolution, confined growth, etc. Fractal properties are found to play a role in catalysis and chromatography and in sol-gel synthesis, dendritic growth, leaching, and fracturing. Various numerical strategies can mimic these growth processes in 2D or in 3D.

Two interesting properties of fractal pore network are worth mentioning in this short presentation. First, to tile the fractal matrix with a collection of yardsticks having a typical size ε, the total number of yardsticks needed to cover the all object is proportional to ε^{-d_f}. Here d_f is the fractal dimension ranging between 0 and 3. Secondly, for a self-similar structure, the mass contained inside a box of size L evolves as L^{d_f}.

Fractal geometry can be applied in numerous cases. However, some hierarchical textures having specific organization at different length scale are still difficult to describe as a "whole". This is the case, for example, for carbonate rocks, geological porous formations, and numerous porous biological tissues (bone, biofilm, skin). The need to find adequate tools to handle the stochastic multiscale complexity is a challenging issue for the future.

9. MACROPOROUS REFERENCE MATERIALS

9.1 Introduction

Gas adsorption and mercury porosimetry are now widely used as standard methods for the characterization of porous materials, which are of great importance in many areas of industry and technology. Over the past 10 years, the quality management requirements in testing laboratories according to ISO 17025 [84] have brought about an increased demand for RMs for both methods. According to the new definition approved at the 2005 Annual Meeting of ISO REMCO (the Committee on Reference Materials of the International Organization for Standardization) [85], an RM is a material that is sufficiently homogeneous and stable with respect to specified properties and that has been established to be fit for its intended use in a measurement process. The properties can be quantitative or also qualitative, e.g., identity of substances or species. A certified reference material (CRM) is an RM that is characterized by a metrologically valid procedure for one or more specified properties, accompanied by a certificate that provides the value of the specified property, its associated uncertainty, and a statement of metrological traceability. This means that CRMs are a subgroup of RMs. Each certified value of a CRM must be accompanied by a statement of its uncertainty summed up in the certificate, otherwise the material cannot be regarded as a CRM. The uncertainty indicates the range where the "true" property value can be expected with a stated probability. The uncertainty statement is one reason why CRMs are of higher metrological quality than non-CRMs, the other is that CRMs are usually certified by a recognized authority, such as national metrology institutes (NMIs) or national testing institutes. Furthermore, to control their products and to calibrate their instruments, many manufacturers of powders or porous materials produce internal RMs for their own needs.

To meet the requirements for their role as quantitative scales, which make possible the transfer of the values of measured or assigned quantities between one place and another, RMs must be sufficiently homogeneous and stable. The characterization of the property values must have been performed using suitable, well-described, and validated methods. If possible, standardized methods should be used.

There are various guidelines concerning the development and certification of RMs as prepared by ISO REMCO, the international committee for RMs [86–92].

9.2 Special issues raised by macroporous RMs

Macroporous materials, like any other porous RM, raise several issues which must be addressed, namely:

- In contrast to bulk metals, inorganic oxides, or organic substances for which any sample of high and known purity can play the part of an RM as defined above, there is no macroporous RM readily available with pore sizes, say, in the 50 nm to 50 μm range.
- Problems of homogeneity and representative sampling are critical.
- The stability of the porous structure should be checked, especially for the materials which were freshly prepared in order to be tailored with the pore size of interest.

It may be difficult, therefore, to prepare a reliable macroporous RM in an institution, which is otherwise specialized in the production of RMs, and it turns out that at present only a few certified macroporous reference materials (CMRMs) are available (see [86]).

In contrast to other kinds of RMs, the development and certification of porous RMs is characterized by some special features. The most commonly measured physical dimensional parameters of macroporous solids are mean pore size and total specific pore volume. At the moment, only a small fraction of the different measuring methods based on the principle of intrusion has been standardized. Indeed, some of the methods in current use do not have the theoretical basis that allows the calculation of quantitative results. As a consequence, there are problems with the comparability of methods based on totally different physical principles, and very often a dependence of the results of porosity measurements upon the method used (including the selected pore model) can be observed. Further difficulties result from the fact that the pore system of a solid may be sensitively influenced by different kinds of sample pretreatment. This is, however, also the case for quite a lot of other procedures for materials properties measurement. Therefore, the necessity of standardization not only of the experimental procedures (including sampling) used for porosity studies but also of the computational algorithms for calculating the results and derived quantities is another point of importance for the certification of porous RMs. This also includes questions of stability and homogeneity testing as well as various aspects of the statistical treatment of interlaboratory tests and the estimation of uncertainty budgets for porous CRMs.

As the certified value of a porous CRM is method-dependent, there is no direct traceability for the certified values in the sense of the *Vocabulary of International Metrology* (*VIM*) [86] that defines traceability as a property of the result of a measurement or the value of a standard, whereby it can be related to a reference through a documented unbroken chain of calibrations, each contributing to the measurement uncertainty. Consequently, the certified values of existing porous CRMs are not directly traceable to such internationally accepted standards, preferably to the basic units of the International System of Units (SI). Instead, these materials are artifacts representing the end-point of the traceability chain and define the scale of porosity measurement. At this stage, the only possible way for the certification of porous RMs consists in value assignment on the basis of the statistical evaluation of interlaboratory comparison studies with selected technically competent laboratories as participants. It is assumed that in this way possible undetected systematic errors, leading to positive and negative biases, can be leveled.

9.3 Current availability of macroporous CRMs worldwide

Since the major method used to characterize macroporous materials is still mercury porosimetry, this is the method for which the few macroporous CRMs available in the world were certified. These CRMs can be found under several trademarks, especially:

- BAM, which stands for the German Federal Institute for Materials Research and Testing;
- SRM®, which is a trademark registered by the U.S. National Institute for Standards and Technology (NIST) for the CRMs they produce and stands for standard reference material; and
- ERM®, which is a trademark of the European Communities for CRMs produced by partners of the European Reference Material (ERM) cooperation and fulfilling stringent quality criteria.

The current worldwide availability of CMRMs is summarized in Table 1 from which can be seen that only very few CRMs for intrusion methods are available at the moment. Among these materials are aluminas, alumina ceramics, silica-alumina, and porous glasses. Their certified pore sizes and pore volumes cover ranges from about 9 nm to 5.8 μm and (0.1 to 0.9) cm^3·g^{-1}, respectively. They are intended for testing the performance of mercury porosimeters and for the improvement of quality assurance in pore size analysis laboratories. In addition, with certain limitations, the care brought to prepare, sample, homogenize, store, and keep available such CRM,s can make them also valuable for *inter-comparison of methods,* for which they were not certified, provided they withstand the particular experimental conditions.

Table 1 Currently available CRMs for intrusion methods.

Material	Order number	Certified and distributed by	Method used	Mean pore diameter		Pore volume	
				Certified value (nm)	Uncertainty (nm)	Certified value ($cm^3 \cdot g^{-1}$)	Uncertainty ($cm^3 \cdot g^{-1}$)
α-Alumina	ERM®-FD120	BAM	MIP	228.0	5.9[a]	0.548	0.013[a]
Porous glass	ERM®-FD121	BAM	MIP	15.1	0.2[a]	0.625	0.002[a]
Porous glass	ERM®-FD122	BAM	MIP	139.0	3.7[a]	0.924	0.002[a]
Alumina ceramics	ERM®-FD123	BAM	MIP	3052	153[a]	0.100[c]	0.004[a]
Alumina ceramics	BAM-P124	BAM	MIP	3074	185[b]	0.158[c]	0.007[b]
Alumina ceramics	BAM-P125	BAM	MIP	5797	216[b]	0.208[c]	0.01[b]
Alumina ceramics	BAM-P126	BAM	MIP	1746	86[b]	0.111[c]	0.009[b]
Alumina	BAM-P127/ SRM 1917	BAM & NIST	MIP	23.86	0.52[a]	0.639[c]	0.004[a]
Silica-alumina	SRM 1918	NIST	MIP	8.847	0.363[a]	0.547	0.018[a]
Alumina	SRM 1917/ BAM-P127	NIST& BAM	MIP	23.86	0.52[a]	0.639[c]	0.004[a]

[a]Expanded uncertainty $U = ku_c$ (95 % level of confidence, coverage factor $k = 2$), where u_c is a combined standard uncertainty for the average, calculated according to *the ISO Guide to the Expression of Uncertainty* [93].
[b]Half width of the 95 % confidence interval.
[c]Material with certified volume values of the whole mercury intrusion (pressure/volume) curve.
MIP: mercury intrusion porosimetry
BAM: Bundesanstalt für Materialforschung und -prüfung, Richard-Willstätter-Str. 11, D-12489 Berlin, Germany,
NIST: National Institute of Standards and Technology, Gaithersburg, MD 20899-0001, USA, <www.nist.gov/srm/>
ERM: European Reference Material, besides from BAM also available from <www.erm-crm.org/ermcrmdb/jsp/default.jsp>

A special feature of the CRMs for the mercury porosimetry method developed at BAM in Germany (and in one case together with NIST in the USA) is the certification of the whole mercury intrusion curve (pore volume as a function of intrusion pressure) instead of certifying only single values of certain properties such as the mean pore width or the pore volume. The advantage of such certification consists in the availability of a large set of certified data points in the working range of a typical porosimeter between 0.1 and 400 MPa and the independence of any evaluation model such as Washburn's equation, etc. The comparison between the measured and the certified intrusion curves (e.g., by means of plotting both curves overlaid in one diagram) enables the user to check the volume calibration of the porosimeter as well as the condition of the pressure transducer.

9.4 Future work in the field of macroporous CRMs for intrusion methods

Future work is necessary to develop macroporous RMs for various pore size characterization methods, other than gas adsorption and mercury porosimetry. Another important task is the development of macroporous RMs with preferably uniform pore systems as a basis for comparing the various measuring methods with each other (materials with the function of common yardsticks for calibrating different methods). The advantage of macroporous materials with uniform, regularly shaped pores with sizes of about 1 µm or more would consist, for instance, in the possibility of direct and independent characterizing and visualizing the pores by means of imaging techniques such as X-ray microtomography, scanning electron microscopy (SEM), environmental scanning electron microscopy (ESEM), or optical microscopy in combination with image analysis. Unfortunately, upscaling reproducible syntheses for such macroporous materials to yield a sufficiently large amount of the material with appropriate stability and homogeneity remains an unsolved problem. From the theoretical point of view, a clearer definition of the terms describing porosity properties of real pore systems is necessary, e.g., specifying the

pore size in the case of real irregularly shaped pores. This is an important prerequisite for the harmonization and standardization of measuring methods in the field of macropore characterization based on different physical principles and for the development and certification of adequate RMs certified using more than one characterization method. It would also be an advance in the development of better scales for porosity parameters.

10. CONCLUSIONS

Each of the experimental methods described above has particular advantages and limitations, which are dependent on its underlying principles and the nature and complexity of the macropore structure. It follows that no method should be expected to give a definitive evaluation of the macropore size distribution.

The most suitable characterization method depends on the intended use of the macroporous material and the physical phenomena involved. For example, if the material is to be used as a filter, a membrane, or a porous plug, it is evident that *fluid permeation methods* are the most appropriate.

At present, mercury porosity is the most widely used technique for the characterization of a variety of macroporous solids (e.g., catalysts and building materials). The commercial equipment now available is generally regarded as user-friendly and capable of providing reliable intrusion–extrusion data on a routine basis over a wide range of macropore (and mesopore) size. The limitations are well documented, and it is understood that the interpretation of the intrusion data is not always straightforward. Furthermore, *specific safety measures* must be taken, as discussed in Section 2.4.

For a number of reasons, *liquid or contact porosimetry and water desorption calorimetry* are promising alternative methods and worthy of refinement for the comparative assessment of *pore volume* and *pore size distribution.*

Although the pore volume and pore size distribution are usually regarded as basic parameters of a pore structure, they are often of very limited value. A much more elaborate description of porous networks is necessary *to gain an understanding of the mechanisms of synthesis or the behaviour of macroporous materials or to be able to extend the range of their applications.* One then needs to present the relevant properties of pore networks in a 3D form.

To achieve these aims, it will be essential to apply *several experimental methods of characterization together with advanced modeling procedures.* In addition to the improvement of existing methods (with the help of porous RMs), it will be necessary *to look for new ones,* based on methodology and physical phenomena that are not yet exploited for this purpose.

MEMBERSHIP OF SPONSORING BODY

Membership of the IUPAC Physical and Biophysical Chemistry Division Committee for the period 2010–2011 was as follows:

*President***:** A. J. McQuillan (New Zealand); *Vice President***:** K. Yamanouchi (Japan); *Secretary***:** R. Marquardt (France); *Past President***:** M. J. Rossi (Switzerland); *Titular Members***:** J. H. Dymond (UK); A. Friedler (Israel); R. Guidelli (Italy); J. Hou (China); B. D. Sykes (Canada); A. K. Wilson (USA); *Associate Members***:** V. Barone (Italy); K. Bartik (Belgium); A. R. H. Goodwin (USA); V. Mišković-Stanković (Serbia); G. R. Moore (UK); M. Rico (Spain); *National Representatives***:** K. Bhattacharyya (India); S.-J. Kim (Korea); V. Yu. Kukushkin (Russia); A. J. Mahmood (Bangladesh); O. V. Mamchenko (Ukraine); F. H. Quina (Brazil); Á. W. Mombrú Rodríguez (Uruguay); N. Soon (Malaysia); V. Tsakova (Bulgaria); M. Witko (Poland).

REFERENCES

1. K. S. W. Sing, D. H. Everett, R. A. W. Haul, L. Moscou, R. A. Pierotti, J. Rouquerol, T. Siemieniewska. *Pure Appl. Chem.* **57**, 603 (1985).
2. J. Rouquerol, D. Avnir, C. W. Fairbridge, D. H. Everett, J. R. Haynes, N. Pernicone, J. D. F. Ramsay, K. S. W. Sing, K. K. Unger. *Pure Appl. Chem.* **66**, 1739 (1994).
3. H. Giesche. In *Handbook of Porous Solids*, Vol. 1, F. Schueth, K. S. W. Sing, J. Weitkamp (Eds.), pp. 309–351, Wiley-VCH, Weinheim (2002).
4. C. León y León. *Adv. Colloid Interface Sci.* **76–77**, 341 (1998).
5. ISO 15901-1:2005, "Pore size distribution and porosity of solid materials by mercury porosimetry and gas adsorption – Part 2: Analysis of macropores by mercury porosimetry", International Organization for Standardization (ISO), Geneva (2005).
6. S. Lowell, J. Shields, M. A. Thomas, M. Thommes. *Characterization of Porous Solids and Powders: Surface Area, Porosity and Density*, Springer (2004).
7. C. Felipe, S. Cordero, I. Kornhauser, G. Zgrablich, R. Lopez, F. Rojas. *Part. Part. Syst. Charact.* **23**, 48 (2006).
8. S. P. Rigby, I. O. Evbuoumwan, M. J. Watt-Smith, K. Edler, R. S. Fletcher. *Part. Part. Syst. Charact.* **23**, 82 (2006).
9. (a) F. Porcheron, P. A. Monson, M. Thommes. *Langmuir* **20**, 6482 (2004); (b) F. Porcheron, M. Thommes, R. Ahmad, P. A. Monson. *Langmuir* **23**, 3372 (2007).
10. U.S. Department of Labor Occupational Safety and Health Administration (OSHA), Safety and Health Topics: Health Guidelines (2010). <http://www.osha.gov/SLTC/mercury/exposure_limits.html>
11. U.S. Department of Labor Occupational Safety and Health Administration (OSHA). *Occupational Safety and Health Guideline for Mercury Vapor*, September (1996). <http://www.osha.gov/SLTC/healthguidelines/mercuryvapour/recognition.html>
12. National Institute for Occupational Safety and Health (NIOSH). Publication No. 92-100 (1992). <http://www.cdc.gov/niosh/pdfs/92-100.pdf>
13. J. D. Blando, D. Singh. *Controlling Metallic Mercury Exposure in the Workplace: A Guide for Employers*, revised ed., New Jersey Department of Health and Senior Services, Trenton, NJ (2004). <http://www.state.nj.us/health/surv/documents/mercemp.pdf>
14. F. Gomez, R. Denoyel, J. Rouquerol. *Langmuir* **16**, 3474 (2000).
15. B. Lefevre, A. Saugey, J.-L. Barrat, L. Bocquet, E. Charlaix, P. F. Gobin, G. Vigier. *J. Chem. Phys.* **120**, 4927 (2004).
16. A. Jena, K. Gupta. *Fluid Particle Separation J.* **4**, 227 (2002).
17. A. Y. Fadeev, V. Eroshenko. *J. Colloid Interface Sci.* **187**, 275 (1997).
18. V. Eroshenko, R.-C. Regis, M. Soulard, J. Patarin. *J. Am. Chem. Soc.* **123**, 8129 (2001).
19. B. Miller, I. Tyomkin. *J. Colloid Interface Sci.* **162**, 163 (1994).
20. Yu. M. Volfkovitch, V. S. Bagotzky, V. E. Sosenkin, E. I. Shkolnikov. *Sov. Electrochem.* **16**, 1325 (1981).
21. Yu. M. Volfkovitch, V. S. Bagotzky, V. E. Sosenkin, I. A. Blinov. *Colloids Surf., A* **187–188**, 349 (2001).
22. A. V. Neimark. *Ads. Sci. Technol.* **7**, 210 (1990).

23. A. V. Neimark. *JETP Lett.* **51**, 535 (1990).
24. A. V. Neimark, E. Robens, K. K. Unger, J. M. Volfkovich. *Fractals* **2**, 45 (1994).
25. P. N. Aukett, C. A. Jessop. In *Fundamentals of Adsorption*, M. D. Le Van (Ed.), p. 59, Kluwer, Boston (1996).
26. K. L. Muray, N. A. Seaton, M. A. Day. *Langmuir* **15**, 6728 (1999).
27. R. Denoyel, M. Barrande, I. Beurroies. In *Studies in Surface Science and Catalysis*, P. Llewellyn et al. (Eds.), Elsevier, **160**, 33 (2007).
28. I. Gusev. *J. Chromatogr., A* **855**, 273 (1999).
29. P. C. Carman. *Trans. Inst. Chem. Eng.* **15**, 150 (1937).
30. S. Mauran. *Transport Porous Media* **43**, 355 (2001).
31. V. Kapur. *Ind. Eng. Chem. Res.* **35**, 3179 (1996).
32. F. C. Leinweber. *Anal. Chem.* **74**, 2470 (2002).
33. F. C. Leinweber. *J. Chromatogr., A* **1006**, 207 (2003).
34. F. C. Leinweber. *Chem. Eng. Technol.* **11**, 1177 (2002).
35. N. Vervoort. *Anal. Chem.* **75**, 843 (2003).
36. P. Gzil. *Anal. Chem.* **76**, 6707 (2004).
37. A. F. Miguel, A. Serrenho. *J. Phys. D: Appl. Phys.* **40**, 6824 (2007).
38. R. Skudas, B. A. Grimes, M. Thommes, K. K. Unger. *J. Chromatogr., A* **1216**, 2635 (2009).
39. M. Brun, J. F. Quinson, C. Eyraud. *Thermochim. Acta* **21**, 59 (1977).
40. M. Barrande, I. Beurroies, R. Denoyel, I. Tatarova, M. Gramblicka, M. Polakovic, M. Joehnck, M. Schulte. *J. Chromatogr., A* **1216**, 6906 (2009).
41. J. H. Strange, M. Rahman, E. G. Smith. *Phys. Rev. Lett.* **71**, 3589 (1993).
42. D. Vargas-Florencia, O. V. Petrov, I. Furo. *J. Colloid Interface Sci.* **305**, 280 (2007).
43. M. P. Hollewand, L. F. Gladden. *J. Catal.* **144**, 254 (1993).
44. (a) Y. Wang, F. De Carlo, D. C. Mancini, I. McNulty, B. Tieman, J. Bresnahan, I. Foster, J. Insley, P. Lane, G. von Laszewski, C. Kesselman, M. H. Su, M. Thiebaux. *Rev. Sci. Instrum.* **72**, 2062 (2001); (b) J. H. Raistrick. *Mater. World* **9**, 11 (2001).
45. J. H. Raistrick. *Mater. World* **9**, 11 (2001).
46. A. J. Koster, U. Ziese, A. J. Verklejj, A. H. Janssen, K. P. de Jong. *J. Phys. Chem. B* **104**, 9368 (2000).
47. L. Holzer, F. Indutnyi, P. H. Gasser, B. Munch, M. Wegmann. *J. Microsc.* **216**, 84 (2004).
48. J. T. Fredrich. *Phys. Chem. Earth A* **24**, 551 (1999).
49. P. T. Callaghan. *Principles of Nuclear Magnetic Resonance Microscopy*, Clarendon Press, Oxford, UK (1991).
50. L. Ruffino, R. Mann, R. Oldman, E. H. Stitt, E. Boller, P. Cloetens, M. di Michiel, J. Merino. *Can. J. Chem. Eng.* **83**, 132 (2005).
51. S. P. Rigby, M. J. Watt-Smith, P. Chigada, J. A. Chudek, R. S. Fletcher, J. Wood, S. Bakalis, T. Miri. *Chem. Eng. Sci.* **61**, 7579 (2006).
52. S. P. Rigby, R. S. Fletcher. *Part. Part. Syst. Charact.* **21**, 138 (2004).
53. S. Torquato. *Random Heterogeneous Materials: Microstructure and Macroscopic Properties*, Springer, New York (2005).
54. P. Levitz. In *Handbook of Porous Solids*, Vol. 1, F. Schueth, K. S. W. Sing, J. Weitkamp (Eds.), Chap. 2, Wiley-VCH, Weinheim (2002).
55. F. A. Dullien. *Porous Media: Fluid Transport and Pore Structure*, Academic Press, New York (1976).
56. M. Sahimi. *Flow and Transport in Porous Media and Fractured Rock*, VCH (1995).
57. J. Serra. *Image Analysis and Mathematical Morphology*, Academic Press, London (1982).

58. S. Ryde, S. Anderson, K. Larson, Z. Blum, T. Landh, S. Lidin, B. W. Ninham. *The Language of Shape: The Role of Curvature in Condensed Matter*, Elsevier (1997).
59. C. H. Arns, M. A. Knackstedt, K. R. Mecke. *Colloids Surf., A* **241**, 351 (2004).
60. B. Lu, S. Torquato. *J. Chem. Phys.* **93**, 3452 (1990).
61. R. Hilfer. *Phys. Rev. B* **44**, 60 (1991).
62. B. Biswal, C. Manwart, R. Hilfer. *Physica A* **255**, 221 (1998).
63. P. Levitz, D. Tchoubar. *J. Phys. I* **2**, 771 (1992).
64. P. Levitz. In *Characterisation of Porous Solid IV*, B. McEnaney et al. (Eds.), p. 213, Royal Society of Chemistry (1997).
65. M. Coleman. *J. Appl. Prob.* **2**, 169 (1965).
66. H. Reiss. *J. Phys. Chem.* **96**, 4736 (1992).
67. M. Doi. *J. Phys. Soc. Jpn.* **40**, 567 (1976).
68. A. Guinier, G. Fournet. *Small Angle Scattering of X-rays*, Chap. 1, John Wiley (1955).
69. L. K. Barrett, C. S. Yust. *Metallography* **3**, 1 (1970).
70. C. Lin, M. H. Cohen. *J. Appl. Phys.* **59**, 328 (1994).
71. L. Pothuaud, P. Porion, E. Lespessailles, C. L. Benhamou, P. Levitz. *J. Microsc.* **199**, 149 (2000).
72. M. Han, S. Youssef, E. Rosenberg, M. Fleury, P. Levitz. *Phys. Rev. E* **79**, 031127 (2009).
73. L. Pothuaud, B. Rietbergen, L. Mosekilde, O. Beuf, P. Levitz, C. Benhamou, S. Majumdar. *J. Biomechan.* **35**, 1091 (2002).
74. D. Stoyan, W. Kendall, J. Mecke. *Stochastic Geometry and its Applications*, 2nd ed., John Wiley (1995).
75. M. Y. Joshi. Ph.D. thesis, University of Kansas, USA (1974).
76. P. M. Adler, C. G. Jacquin, J. A. Quiblier. *Int. J. Multiphase Flow* **16**, 691 (1990).
77. P. Levitz. *Adv. Colloid Interface Sci.* **76–77**, 71 (1998).
78. R. D. Hazlett. *Math. Geol.* **29**, 801 (1997).
79. M. Rintoul, S. J. Torquato. *Colloid Interface Sci.* **186**, 467 (1997).
80. C. L. T. Yeong, S. Torquato. *Phys. Rev. E* **57**, 495 (1998).
81. C. L. T. Yeong, S. Torquato. *Phys. Rev. E* **58**, 224 (1998).
82. B. B. Mandelbrot. *The Fractal Geometry of Nature*, W.H. Freeman, San Francisco (1982).
83. J. F. Gouyet. *Physics and Fractal Structures*, Springer (1996).
84. ISO/IEC 17025:2005, *General Requirements for the Competence of Testing and Calibration Laboratories*, International Organization for Standardization (ISO), Geneva (2005).
85. H. Emons, A. Fajgelj, A. M. H. van der Veen, R. Watters. *Accred. Qual. Assur.* **10**, 576 (2006).
86. ISO/IEC Guide 99, *International Vocabulary of Metrology - Basic and General Concepts and Associated Terms* (*VIM*), 3rd ed. (2007). JCGM 200:2008 at <http://www.bipm.org/en/publications/guides/vim>
87. ISO Guide 30:1992, *Terms and Definitions Used in Connection with Reference Materials*, International Organization for Standardization (ISO), Geneva (1992).
88. ISO Guide 31:2000, *Contents of Certificates of Reference Materials*, International Organization for Standardization (ISO), Geneva (2000).
89. ISO Guide 32:1997, *Calibration of Chemical Analysis and Use of Certified Reference Materials*, International Organization for Standardization (ISO), Geneva (1997).
90. ISO Guide 33:2000, *Uses of Certified Reference Materials*, International Organization for Standardization (ISO), Geneva (2000).
91. ISO Guide 34:2000, *General Requirements for the Competence of Reference Material Producers as Amended by Technical Corrigendum 1 of 15/11/2003*, International Organization for Standardization (ISO), Geneva (2003).

92. ISO Guide 35:2006, *Certification of Reference Materials: General and Statistical Principles*, International Organization for Standardization (ISO), Geneva (2006).

93. ISO/IEC Guide 98:1995, *Guide to the Expression of Uncertainty in Measurement (GUM)*, International Organization for Standardization (ISO), Geneva (1995).